JACS
JOURNAL OF THE AMERICAN CHEMICAL SOCIETY

Article

pubs.acs.org/JACS

Dynamic Behavior of DNA Cages Anchored on Spherically Supported Lipid Bilayers

J. W. Conway, C. Madwar, T. G. Edwardson, C. K. McLaughlin, J. Fahkoury, R. B. Lennox, and H. F. Sleiman*

Department of Chemistry, McGill University, 801 Sherbrooke Street West, Montreal, Quebec H3A 0B8, Canada

Supporting Information

ABSTRACT: We report the anchoring of 3D-DNA-cholesterol labeled cages on spherically supported lipid bilayer membranes (SSLBM) formed on silica beads, and their addressability through strand displacement reactions, controlled membrane orientation and templated dimerization. The bilayer-anchored cages can load three different DNA-fluorophores by hybridization to their "top" face (furthest from bilayer) and unload each of them selectively upon addition of a specific input displacement strand. We introduce a method to control strand displacement from their less accessible "bottom" face (closest to the bilayer), by adding cholesterol-substituted displacing strands that insert into the bilayer themselves in order to access the toehold region. The orientation of DNA cages within the bilayer is tunable by positioning multiple cholesterol anchoring units on the opposing two faces of the cage, thereby controlling their accessibility to proteins and enzymes. A population of two distinct DNA cages anchored to the SSLBMs exhibited significant membrane fluidity and have been directed into dimer assemblies on bilayer via input of a complementary linking strand. Displacement experiments performed on these anchored dimers indicate that removal of only one prism's anchoring cholesterol strand was not sufficient to release the dimers from the bilayer; however, removal of both cholesterol anchors from the dimerized prisms via two displacement strands cleanly released the dimers from the bilayer. This methodology allows for the anchoring of DNA cages on supported lipid bilayers, the control of their orientation and accessibility within the bilayer, and the programmable dimerization and selective removal of any of their components. The facile coupling of DNA to other functional materials makes this an attractive method for developing stimuli-responsive protein or nanoparticle arrays, drug releasing biomedical device surfaces and self-healing materials for light harvesting applications, using a highly modular, DNA-economic scaffold.

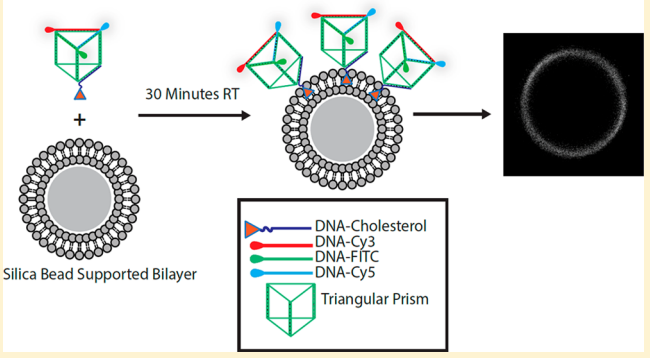

INTRODUCTION

DNA nanostructures have shown tremendous promise for the precise organization of functional materials.[1] In order to integrate them into devices for diagnostic assays,[2] optoelectronic,[3] plasmonic circuitry[4] or biomedical applications,[5,6] it will be important to transition these structures from solution to solid surfaces. DNA structures have been typically immobilized on hard surfaces (such as gold or silicon),[1b,7] but these rigid surfaces diminish or completely shut down the 2D-diffusion of tethered DNA and serve as a significant steric and diffusion barrier. On the other hand, lipid bilayers present a soft, fluid two-dimensional substrate that can effectively interface with numerous solid substrates.[1d,8] Anchoring DNA nanostructures to these bilayers may preserve their dynamic character, and depending on the lipid composition and experimental conditions, would allow 2D-motion of these structures with tunable kinetics.

DNA strands positioned on lipid membranes have been used in a variety of contexts. They can act as tethers of lipid vesicles to planar bilayers,[9] as mediators of vesicle fusion in analogy to SNARE proteins,[10] as guides for the formation of "designer" microtissues from DNA tagged cells,[11] and as templates for the formation of supramolecular vesicle networks.[10] DNA nanostructures anchored in lipid membranes have been shown to mimic the behavior of nanopore forming proteins[12] and the properties of photosynthetic systems.[1a,13] Peptide nucleic acid-DNA hybrid structures can cluster in specific lipid domains, and this clustering can be changed to other domains with the addition of nucleases that degrade the DNA component.[14] Two studies have recently examined dynamic behavior of 2D-DNA origami structures on lipid bilayers, by photochemically switching the association of hexagonal origami tiles, or by hybridization of origami "barges" that are held at a distance from the lipid bilayer membrane.[15] Another study using cholesterol functionalized DNA origami helical bundles examined the dynamics of these structures on free-standing

Received: June 17, 2014
Published: August 20, 2014

   dx.doi.org/10.1021/ja506095n | J. Am. Chem. Soc. 2014, 136, 12987−12997

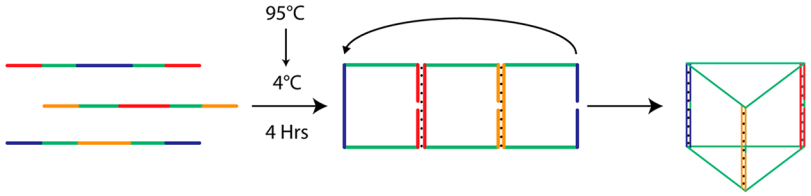

Figure 1. Clip-by-clip assembly of TP scaffold.

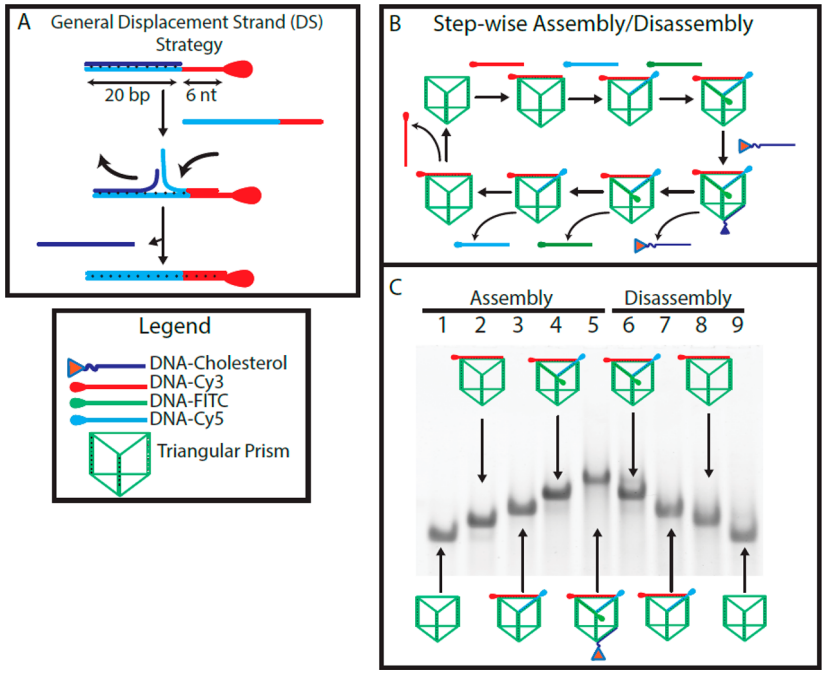

Figure 2. (A) Schematic representation of the displacement strategy. (B) Representation of the stepwise assembly/disassembly on a DNA triangular prism scaffold. (C) Nondenaturing polyacrylamide gel electrophoresis showing the stepwise addressability of the triangular DNA scaffold and its disassembly via strand displacement. Lane 1: TP scaffold, lane 2: previous + Cy3, lane 3: previous + Cy5, lane 4: previous + Alexa488 (A488), lane 5: previous + cholesterol anchor, lane 6: previous, displace cholesterol anchor, lane 7: previous, displace A488, lane 8: previous, displace Cy5, lane 9: previous, displace Cy3.

bilayers while varying the buffer salt concentrations, and the consequent domain partitioning.[16]

We here report the association, dynamic behavior, hybridization and lift-off of cholesterol-labeled three-dimensional DNA cages on spherically supported lipid bilayer membranes (SSLBMs) formed on silica beads. The anchored cages present two faces: a "top" accessible face furthest from the bilayer, and a "bottom" face closest to the bilayer. They can readily load different DNA-fluorophores on their top face and selectively unload each of them upon addition of a specific displacing strand. On the other hand, the bilayer membrane provides a steric barrier for the bottom face of the DNA cages nearest the lipid environment. We introduce a method to control the less sterically accessible bottom face, by using displacing DNA strands that can partially insert into the bilayer themselves via cholesterol modification. We show the ability to control the orientation of the cages within the bilayer by varying the position and number of cholesterol substituents, thereby tuning enzyme accessibility to the cages. In chemical terms, the spherical bilayer can serve as a versatile and tunable "protecting group" for DNA nanostructures. Finally, we show the efficient on-bilayer diffusion of DNA cages, as well as their ability to dimerize by hybridization on the lipid bilayer. The resulting dimer prism is doubly anchored to the bilayer. Lifting off one of its two component prisms is not sufficient to release the dimer from the bilayer; however, removing both anchored prisms with two displacement strands cleanly released the dimer from the bilayer. The 3D-structures used here are DNA-minimal, fully dynamic and appear to be intimately coupled to the lipid bilayer, rather than floating on its surface. Because of the ease of coupling DNA to other functional materials, this approach has the potential to produce stimuli-responsive protein arrays, molecule-responsive drug releasing biomedical device surfaces, and self-healing materials for optoelectronic or light harvesting applications.

RESULTS AND DISCUSSION

Design of the DNA Cage and Assembly Strategy. The DNA cages used in these experiments consist of three 96-base DNA strands or "clips". Each clip is designed so that its two 10 base ends are complementary to the back of the next clip, and the third clip is complementary to the back of the first clip. The result is that hybridization of the three strands leads to a closed triangular prism (TP),[17] Figure 1 (see Supporting Information, S−III). This cage possesses 6 single stranded (ss) 20-base binding regions (green) with different sequences. The top ss regions are used to hybridize to DNA strands carrying fluorescent labels (Cy3, Cy5, and Alexa488), while the bottom

dx.doi.org/10.1021/ja506095n | J. Am. Chem. Soc. 2014, 136, 12987−12997

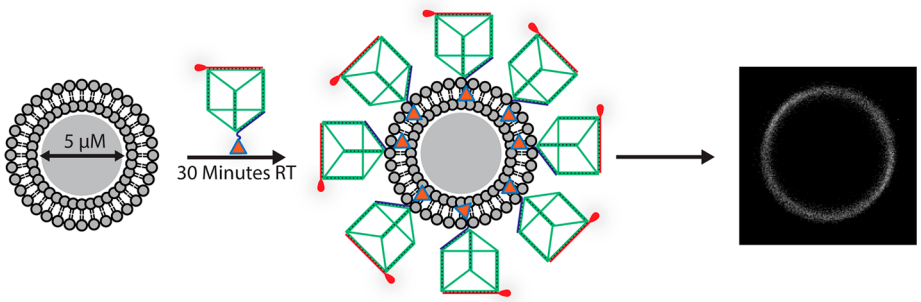

Figure 3. Representation of labeled system (left, not shown to scale) and a confocal fluorescent image of an SSLBM (right).

face hybridizes to a DNA strand that carries a cholesterol anchor. The result is an amphiphilic 3D architecture (Figure 2).

All short oligonucleotides designed to hybridize to the ss regions of the cage consist of the complementary 20 base region followed by a 6-base extension and chemical modification at either the 5′/3′ end (Figure 2). The 6-base extension serves as a toehold initiation point for strand displacement of the 26mer DNA-conjugates from the scaffold. In this way, each of the modified DNA strands can be selectively displaced from the prism by the addition of a strand that is fully complementary to the 26-base stretch (Figure 2A).[17] Using this writing and erasing capability, we will compare the binding and removal of functional DNA-conjugates from a prismatic scaffold in solution and within a lipid bilayer environment.

In Solution Hybridization and Displacement of Fluorescent Labels and Cholesterol Anchors on the DNA Cage. To form the DNA cages, all strands were combined in one pot and annealed from 95 to 10 °C, over 4 h (see Supporting Information, S−III). Assembled structures were characterized by native polyacrylamide gel electrophoresis (Figure 2C). Lane 1 shows a single band corresponding to the assembled DNA cage formed using three 96mer strands, indicating that the prism structure is the single major product formed in near quantitative yield. Lanes 2−5 show the sequential hybridization of the ss regions to three fluorescently labeled DNA strands on the top face and a single cholesterol anchor-substituted strand on the bottom face. The band pattern indicates that the addition of each DNA-conjugate is accompanied by a corresponding decrease in gel mobility. This confirms the formation of the 3D triangular scaffold and successful loading of three different fluorescent tags and the cholesterol anchor unit.

Lanes 6−8 represent the sequential displacement of three bound fluorophore-DNA strands and the cholesterol-DNA in solution using four different displacement strands (DS). In each of these experiments, the fully loaded prism scaffold (lane 5) was used, and the required DSs were added in 3-fold excess relative to the target strand. The mixtures were incubated for 30 min at room temperature. The increase in gel mobility seen in lanes 6−9 corresponds to the stepwise formation of the initial ss DNA cage. In this way the fully functional DNA cage can be assembled and then disassembled using the correct series of chemical inputs.[18]

Anchoring the DNA Cages on the Lipid Bilayer. In this study, we used SSLBMs composed of the synthetic phospholipid 1,2-dioleoyl-*sn*-glycero-3-phosphocholine (DOPC) on 5 μm silica beads, as a model lipid bilayer membrane.[19] Similar lipid bilayer systems have been used as nanovectors,[20] for protein screening,[21] and as artificial supports for inducing functional neural synapse formation.[22] SSLBMs offer many desirable features as biomembrane model systems in comparison to their vesicle counterparts. They have increased mechanical stability and control of particle size and reproducibility. They can also be readily concentrated into a pellet by centrifugation and washed without compromising the membrane integrity. Such manipulations are highly problematic with the related giant unilamellar vesicles (GUVs).[23] In comparison to flat supported bilayer membranes, SSLBMs are considerably easier to manipulate and examine using a variety of microscopy and spectroscopy techniques that are not available for substrates with a planar geometry.[24] Silica beads are also ideal for interfacing with biological systems due to their chemical inertness and biocompatibility.[20,22] Finally, mesoporous silica particles have been used for finely controlled drug release and have been coupled to lipid bilayer membranes.[21b]

Solutions of annealed DNA cages with cholesterol anchors (cholesterol anchor has 20 nt prism binding region and 6 nt toehold (26 nt version)) were combined with the bilayer coated bead solution in buffer. In general, the sample preparation using a large excess of DNA cages ensures that the beads are completely covered in a homogeneous layer of DNA cages as seen in Figure 5. After 15 min of incubation, the beads/DNA were centrifugated to remove any unbound DNA cage or DNA-conjugate (see Supporting Information, S−IV, for preparation details). The amount of functionalized DNA prism bound to the SSLBMs can be determined through fluorescence intensity quantification of the supernatant solution after prism release from the bilayer (see below, and Supporting Information, S−V). It was determined that 5.9×10^{-13} ($\pm 0.2 \times 10^{-13}$) mol of labeled TP were lifted off and collected from the surface of the beads. This represents 4% of the initial amount of DNA cage that was incubated with the SSLBMs; therefore, there is approximately 6.6×10^5 labeled TP/bead or 8.4×10^3 TP/μm^2, based on the size of the SSLBMs. On the basis of the approximate area of each prism, we predicted 4.7×10^4 TP/μm^2. This data implies partial but homogeneous coverage (see Figure 5) of the spherically supported lipid bilayer membranes (SSLBM) with the DNA cages.

Confocal Fluorescence Imaging of 3D DNA Constructs and Membrane Mobility. Figure 3 shows a typical confocal fluorescence image of a DNA prism functionalized with a single fluorophore and cholesterol anchor loaded on the DOPC SSLBM. The image shows a homogeneous distribution of fluorescence intensity within the SSLBM. A series of control samples served to investigate possible off-target membrane interactions from partially assembled functionalized DNA cages as well as the single-stranded fluorophore-labeled oligonucleo-

dx.doi.org/10.1021/ja506095n | J. Am. Chem. Soc. 2014, 136, 12987−12997

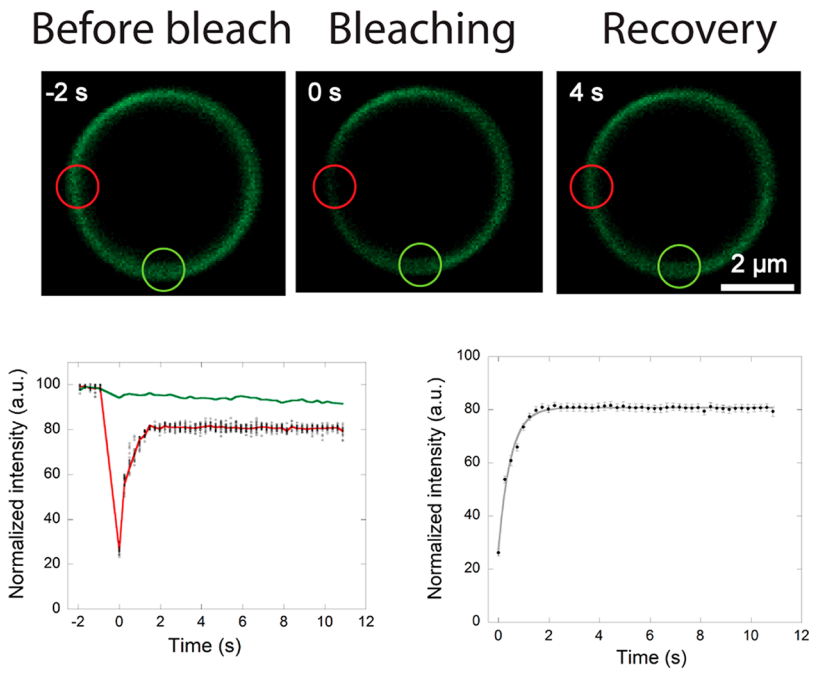

Figure 4. FRAP data. (Top) Images of DOPC SSLBMs containing Alexa488 functionalized DNA cages before and after photobleaching a 1.3 μm spot, indicated by the red circle. A reference spot of the same size indicated by the green circle is used to correct for bleaching caused by imaging. (Bottom left) Individual FRAP data from 20 separate experiments, the averaged FRAP curve of the complete data set of 50 separate experiments (red) and the mean reference curve (green). All FRAP data are normalized to the prebleaching fluorescence. (Bottom right) The averaged FRAP data (and standard error values) fit to a one diffusing component model (R value of 0.994).

tides. In all cases, a measurable and reproducible fluorescence signal is only observed for the fully assembled DNA cage containing both a hybridized fluorophore and cholesterol anchor.

It has been shown that DNA is able to bind to zwitterionic lipid mono/bilayers in the presence of divalent cations.[15b] This work has compared the absorption of the DNA structures to a supported lipid bilayer with and without the cholesterol anchors and has determined that although there are some nonspecific interactions between the DNA and the lipids, the addition of the cholesterol anchors significantly increases the amount of landed DNA structure. Nonspecific binding may also be occurring in our system, but the washing steps during sample preparation minimize this binding. Furthermore, imaging conditions for all beads were kept constant for all samples to allow consistent comparison of fluorescent intensities. It should be noted that at higher laser power some residual fluorescence was observed in the bilayer, and that even after our lift-off experiments (Figure 5) there remains some residual fluorescence on the vesicles. Both of these observations may be attributed to some nonspecific binding of DNA to the lipid bilayer.

The mobility of our prismatic scaffold within the bilayer environment was confirmed using fluorescence recovery after photobleaching (FRAP). Comparative FRAP measurements allow quantification of 2D-diffusion of the DNA cages that are anchored (26 nt version) within the supported lipid bilayers. This involves determining the mobility of a fluorescently labeled DNA cage anchored via cholesterol into a fluid SSLBM lipid membrane formed from DOPC phospholipids (melting point of −20 °C) and comparing it to the mobility of a fluorescent lipid analogue (BODIPY FL-C5) in DOPC SSLBM (see Supporting Information, S−VII).

Figure 4 shows a FRAP study for DOPC SSLBM containing Alexa488-functionalized DNA cages. Recovery of fluorescence intensity was evident, indicating that the DNA cages are mobile and able to diffuse in and out of the bleached spot on a time scale comparable to the control fluorescent lipid molecules (0.472 s for fluorescent DNA conjugates vs 0.377 s for fluorescent lipid analogues). Furthermore, this time scale for fluorescence recovery is in good agreement with previous measurements on labeled SSLBMs.[1d,24b] The values of diffusion coefficients (D), half-life of fluorescence recovery ($\tau_{1/2}$), as well as a ratio of mobile to immobile species are summarized in Table 1.

Table 1. Diffusion Characteristics of Alexa 488 DNA Prism and BODIPY FL-C5 as Measured by FRAP

	Alexa488 DNA Chol	BODIPY FL-C_5
$\tau_{1/2}{}^a$ (s)	0.472	0.377
D^b ($\mu m^2/s$)	0.802	1.00
mobile fraction (%)	80.8 ± 0.2	95.9 ± 0.3

$^a\tau_{1/2}$ is the half-life of fluorescence recovery. ^bD is the diffusion coefficient. For details on fit model equations and calculations of diffusion coefficient, refer to Supporting Information, S−VII.

For the bleached DNA fluorescent conjugate, an average recovery maximum of 80% of the initial fluorescence intensity was observed (taking into account the bleaching caused by imaging). This could be explained by aggregated cholesterol-anchored DNA cages within the supported bilayers contributing to a population of immobile species. Although slightly lower than the values previously reported,[1d,24b,25] which range from 0.6 to 3 $\mu m^2/s$ depending on the sample, our measurements of 0.8 and 1 $\mu m^2/s$ for the prism and lipids are very similar. The difference is likely related to the supported

dx.doi.org/10.1021/ja506095n | J. Am. Chem. Soc. 2014, 136, 12987−12997

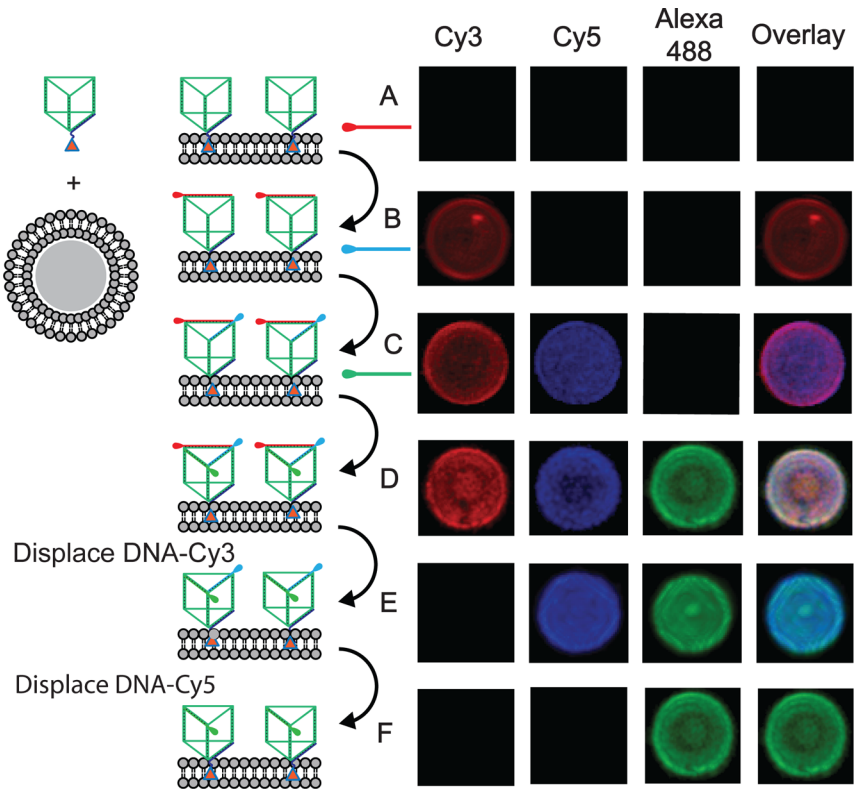

Figure 5. Confocal monitoring of the bilayer during the stepwise assembly and disassembly of the embedded triangular scaffold. Images are Z-stacked 2D images showing the 3D homogeneous morphology of the SSLBMs. Row (A), addition of prism, row (B) Cy3 addition to anchored prisms, row (C) addition of Cy5, row (D) addition of Alexa488, row (E) addition Cy3 displacing strand, row (F) addition of Cy5 displacing strand. Steps A–D represent the assembly; steps E and F represent the disassembly.

bilayer system itself and was not the focus of this study. FRAP analysis was performed using the equation for a 2D diffusion model, which is an approximation for a spherical system. This is usually done for giant unilamellar vesicles as they are large enough that the surface is assumed to be close to planar. This assumption may not be the same for our system (5 μm diameter beads). However, these values are only used for a comparison rather than to report an absolute value. In addition, it is adequate to compare the half-life of recovery for lipids to that for DNA structures, because this value is measured directly and not extrapolated from experiment using diffusion equations. Overall, the similar diffusion characteristics of the fluorescent DNA conjugate to those of the fluorescent lipid analogue in SSLBMs suggest that they undergo similar diffusion kinetics within the SSLBM system.[1d,24b,25]

Stepwise On-Bilayer Hybridization and Strand Displacement from the Top Face of DNA Cages. Many of the existing examples of DNA rearrangements on supported bilayers rely on temperature or enzymatically induced disassembly to initiate domain formation or component partitioning.[14,1c] Strand displacement events on the supported bilayer provide a method to control DNA-mediated membrane interactions using a large number of strand stimuli of different sequences. We thus investigated whether the bilayer anchored DNA cages (26 nucleotide version) would be able to undergo toehold-mediated displacement with added DNA strands. First, we examined lift-off of the strands hybridized to the prism face furthest from the bilayer.

To do this, we prepared SSLBMs and anchored the cholesterol substituted DNA prism as above. We added the three DNA-fluorophore strands (Cy3, Cy5, and Alexa488) sequentially to the bound prisms, each time incubating for 15 min, washing the beads and then collecting them by centrifugation. Figure 5 summarizes the confocal fluorescence images collected after each addition. Rows A–F in Figure 5 show that the DNA cage can be readily hybridized on the supported bilayer membrane to all three of the fluorescent DNA-labels in a stepwise fashion. Confocal images following each incubation step show a homogeneous fluorescent distribution on the bilayer. Overlay images for the sequential labeling additions show colocalization at each step for all fluorophores. This confirms that each prism is able to readily bind several components while associated with a lipid bilayer environment.

We then added the displacement strands to remove the fluorophore labeled oligonucleotides sequentially from the embedded scaffold, as described above. Row E corresponds to the addition of the displacement strand for the DNA-Cy3 component, to the Cy3/Cy5/Alexa488 labeled prisms on the bilayers, followed by washing and centrifugation cycles. Row F corresponds to the same experiment with the displacement strand for the DNA-Cy5 component. Addition of the displacement strand results in the removal of the fluorophore from the anchored DNA cage and complete loss of the fluorescence signal for each corresponding targeted DNA-label. Following removal of the two fluorophores Cy3 and Cy5, only the single Alexa488 fluorophore is observed on the SSLBM surface. This demonstrates that the top face of the DNA cage remains reversibly addressable while incorporated within a SSLBM. Thus, functional components can be organized and selectively lifted off DNA cages anchored on bilayer membrane surfaces.

dx.doi.org/10.1021/ja506095n | J. Am. Chem. Soc. 2014, 136, 12987–12997

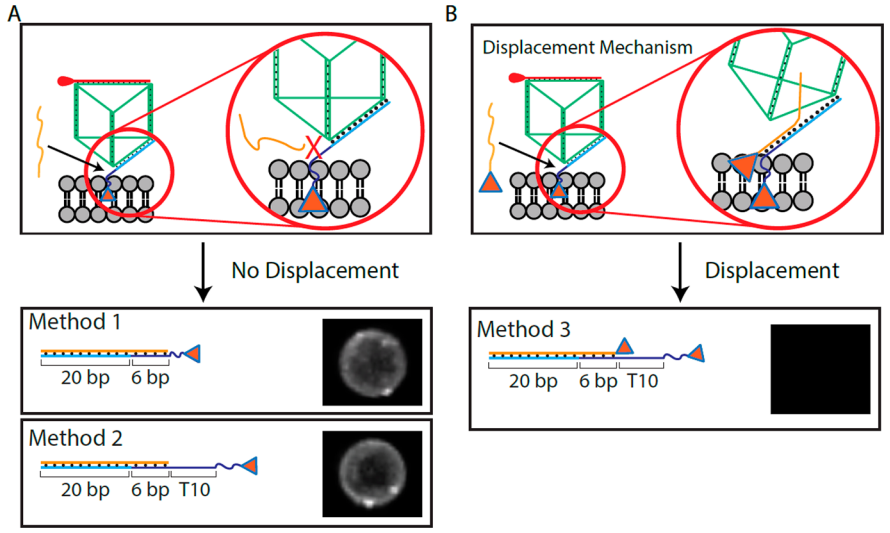

Figure 6. (A) Top, toehold displacement strategies for bottom face strand. (triangle represents cholesterol molecule) Bottom, design of toeholds: Method 1, the cholesterol labeled strand has a 6 base toehold closest to the cholesterol molecule. Method 2, the cholesterol labeled strand has an additional polythymidine (T10 spacer version) between the toehold and cholesterol units. The erasing strand (orange) is unsubstituted. (B) Top, in-bilayer toehold displacement strategy for bottom face strand. The erasing strand (orange) has a cholesterol unit (triangle), allowing it to anchor itself in the bilayer and gain access to the bottom face. Bottom, composition of toehold and erasing strand.

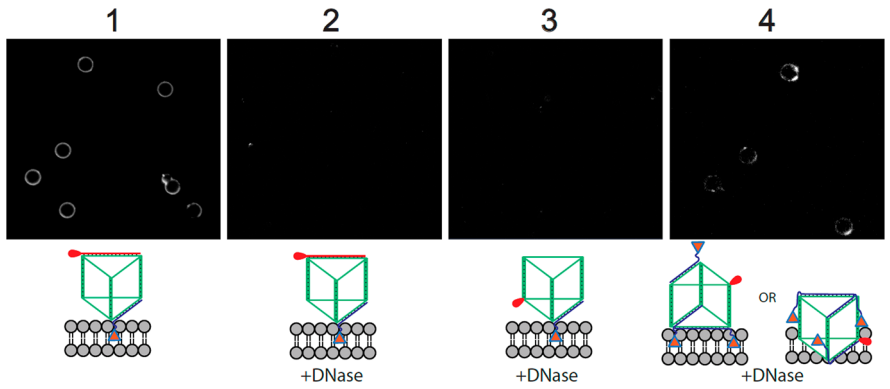

Figure 7. Confocal fluorescent images of the bilayer anchored triangular prism scaffold following DNase I incubation. (1) Hybridized Cy3 label on top face of prism (no DNase I). (2) Hybridized Cy3 label on top face of prism + DNase I. (3) Cy3 label as an internal modification on bottom face of prism + DNase I. (4) Cy3 label as an internal modification +3-Cholesterol anchors on the top and bottom faces of prism + DNase I.

Strand Displacement from the Bottom Face of DNA Cages. Displacement of the cholesterol anchor and subsequent release of the entire DNA cage from the SSLBM surface was examined using a 6 bp toehold region on the DNA-cholesterol strand. This strand displacement would need to occur from the bottom face of the prism which is closest to bilayer, as shown in Figure 6. A triangular prism with a single DNA-Cy5 and a single DNA-cholesterol anchor was incorporated into the SSLBM as described above.

Our initial strategy (method 1, Figure 6A) involved addition of an erasing strand fully complementary to the cholesterol-DNA (26 nt version) strand for 30 min, followed by washing. However, confocal images of the beads following this step displayed unchanged fluorescence intensity. This suggests that the six-base toehold is inaccessible to the displacing strand as it is located directly on the cholesterol anchor, which is embedded within the lipid bilayer. The displacement strand itself can effectively remove the DNA-cholesterol from the prism in solution, as confirmed by native polyacrylamide gel electrophoresis (PAGE) in Figure 2 lane 6.

In a second attempt, we used a DNA-cholesterol anchor containing a polythymidine (T10 version) spacer between the cholesterol unit, and the toehold/binding region (Figure 6A, method 2), in order to distance the toehold from the membrane cholesterol anchor. This modification however yielded similar results and the SSLBMs retained their original fluorescence intensity, indicating that the T10 extension is insufficient to increase the toehold accessibility.

A third strategy (Figure 6B, method 3) proved to be successful. This involves the use of a displacing strand that is itself functionalized with cholesterol, such that it is able to bind to the bilayer, and possibly achieve closer access to the bottom face of the prism. After addition of this cholesterol-DNA strand and washing, SSLBMs with functionalized DNA prism exhibit near complete loss of fluorescence. This confirms that the erasing strand is now able to diffuse into the bilayer, find its complementary binding region and release the entire DNA assembly from the lipid bilayer surface (see below for analysis of the supernatant). Although displacement strategies have previously been used for removal of target strands in a DNA assembly, to our knowledge, this is the first example of a

dx.doi.org/10.1021/ja506095n | J. Am. Chem. Soc. 2014, 136, 12987−12997

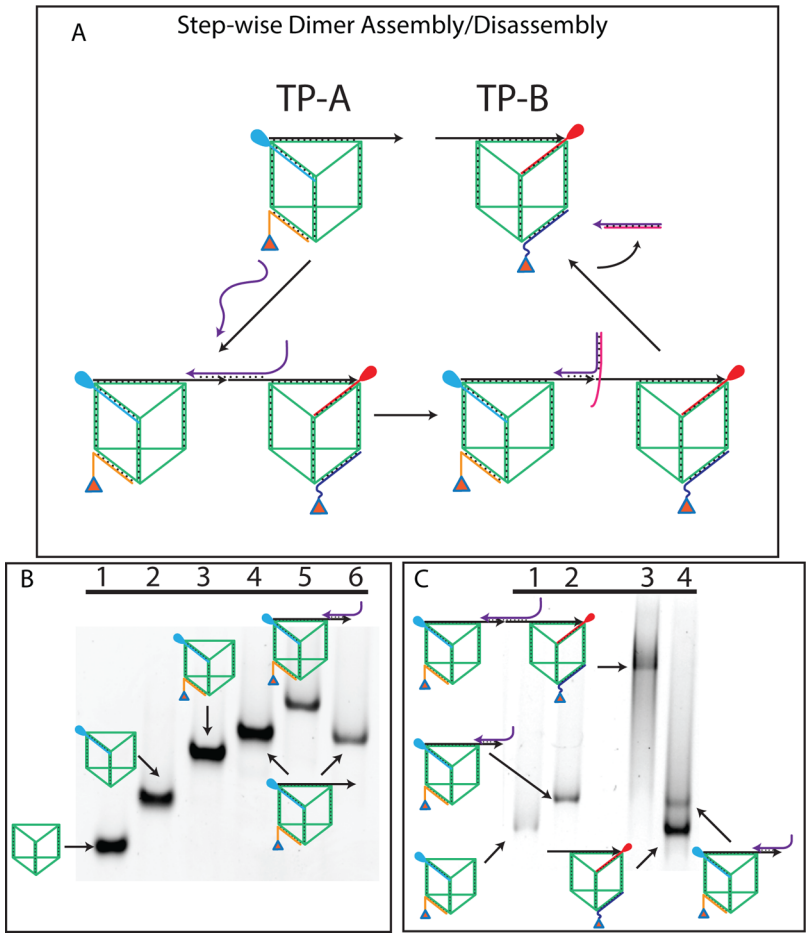

Figure 8. (A) Representation of the stepwise dimer assembly/disassembly. (B) Native PAGE results showing the stepwise loading of the scaffold. Lane 1: TP, lane 2: previous + Cy5 (blue), lane 3: previous + cholesterol anchor (yellow), lane 4: previous + overhang sticky-end (black), lane 5: previous + linking strand (purple), lane 6: previous displace the linking strand. (C) Native PAGE showing stepwise dimer assembly/disassembly. Lane 1: TP-A + Cy5 + cholesterol anchor + overhang, lane 2: TP-B + Cy5 + cholesterol anchor + overhang + linking strand, lane 3: samples in lane 1 and 2 are combined to form the dimer (12 h RT), lane 4: previous + linker displacement to recover monomers.

displacement strategy used within a lipid bilayer system to successfully release a 3D DNA cage. This strategy could not only be used for positioning and control of specific membrane components but could be extended to dynamically and selectively release any DNA macroassemblies that are anchored on a lipid bilayer.

Enzyme Accessibility of DNA Cages on Bilayers. Biological applications using DNA cages assembled on supported bilayers are most likely to involve membrane protein interactions. In order to determine if the DNA scaffolds embedded within the SSLBMs are accessible to enzymatic processing, DNase I, a nonspecific nuclease was added to prisms anchored (T10 spacer version) on this bilayer (30 min followed by washing).

Figure 7 summarizes the results for this assay. Column 1 represents confocal microscopy images of a standard DNA-bead solution before the addition of the nuclease, to confirm homogeneous fluorescent labeling. Column 2 is an image of the same DNA-bead solution containing prisms anchored via the T10 extended cholesterol anchor (see Figure 6), incubated with DNase I. This image shows complete loss of the fluorescence signal, indicating that DNase I is able to interact and digest the membrane bound DNA cages. This is in good agreement with similar studies involving fluorescently labeled duplex DNA constructs.[14]

To determine if only the topmost label binding region of the DNA scaffold is accessible for enzymatic degradation, we assembled a DNA prism containing an internalized Cy3 label, which is oriented on the bottom face of the prism and on the same side as the cholesterol-DNA anchor (T10 spacer version) (see Supporting Information, S−II). Following the enzyme treatment, loss of fluorescence is also observed (Figure 7 column 3), which confirms that indeed the lower portion of scaffold (that is inaccessible to displacement strands, see Figure 6) is being digested and not just the hybridized top label.

Lastly (Figure 7, column 4), the labeled scaffold was again used. However, it was functionalized with 3 cholesterol anchoring units (T10 spacer version), two positioned on the bottom and one positioned on the top face (see Supporting Information, S−II, for DNA sequences). This arrangement of cholesterol units can potentially generate orientations that increasingly bury the DNA scaffold within the membrane, rendering it less accessible to nuclease degradation. There remains a significant amount of fluorescence intensity associated with the bilayer following enzyme incubation (Figure 7, column 4), although it is slightly reduced when compared to the control sample. This indicates that the DNA construct is now only partially accessible to nuclease degradation. Future work will examine the orientation and penetration depth of the DNA cage within the bilayer.

dx.doi.org/10.1021/ja506095n | J. Am. Chem. Soc. 2014, 136, 12987−12997

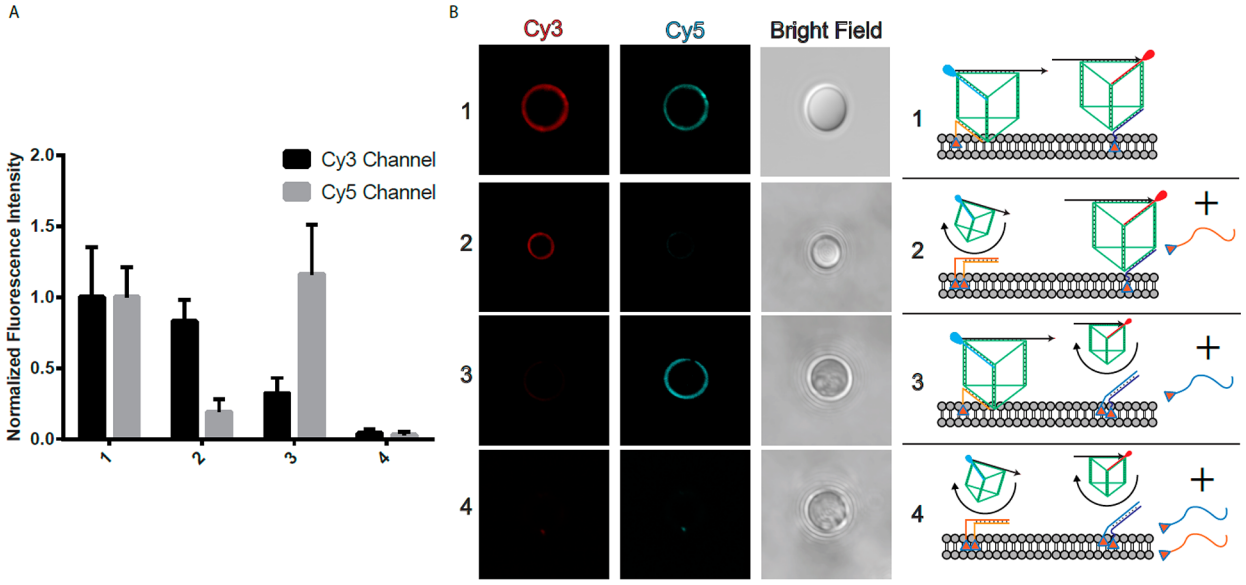

Figure 9. (A) Normalized fluorescence intensity measurements for rows 1 to 4 from (B). (B) Confocal fluorescent images of individual prism bilayer lift-off in a mixed prism population: Row 1: Control sample TP-A(Cy5) + TP-B(Cy3) no linker. Row 2: Displace TP-A (Cy5). Row 3: Displace TP-B (Cy3). Row 4: Displace both prisms.

The modular nature of the DNA cage construction demonstrated here allows for orientational control of the cholesterol units on this scaffold. In turn, this control can be used to tune the position of the DNA cage either on the bilayer surface or deeper within the bilayer. Thus, cages can be more or less accessible to proteins based on their substitution patterns. This may also affect their ability for cellular internalization, when used as drug or oligonucleotide delivery vehicles.

In Solution Dimerization of Prism Scaffolds. To expand the DNA/SSLBM technology for biological and materials applications that require patterning or clustering of these cages on the bilayer, we investigated the reversible dimerization of the DNA cages associated with the bilayer environment. In this regard, we created two prisms (TP-A and TP-B), one functionalized with Cy3 and the second with Cy5 (Figure 8A). Each prism is designed to hybridize a strand containing a 15 base overhang sticky-end, such that an added linking strand can dimerize the two prisms through the overhang components. The linking strand used hybridizes each 15 base overhang, and contains a 5 nt toehold allowing for its dynamic removal from the assembly and consequent dimer dissociation. Each prism is labeled with a unique DNA-cholesterol anchor (T10 spacer version) on the opposite face, and these anchors also contain overhang sequences. Thus, the prisms can individually be removed from the bilayer by using specific displacement strand inputs.

Figure 8B shows the stepwise assembly of all components on the DNA scaffold. Lanes 2, 3, and 4 show the corresponding decrease in gel mobility as the fluorescent tag, cholesterol anchor, and the overhang strand providing the sticky-end are assembled on one of the prisms (TP-A). Lanes 5 and 6 show the addition and consequent displacement of the final linking strand in solution on TP-A (TP-B assembles with the same efficiency, data not shown). In solution, dimerization of TP-A and TP-B is demonstrated in Figure 8C, in which TP-A, prefunctionalized with all components including the linking strand (lane 1), is combined with TP-B, which is also preassembled with all necessary strands except the linking strand (lane 2). Lane 3 represents the dimerization of these two structures following 12 h of incubation at room temperature and shows a band with a corresponding decrease in gel mobility. The linker displacement strand was then added to the assemblies in 2.5 equiv leading to recovery of the initial starting components, as seen in lane 4 by the two bands with comparable mobility to lanes 1 and 2. The diffuse bands in this gel likely arise from lower dimerization efficiency of the two prisms in solution and/or partial dissociation of the TP dimer as it moves down the gel.

Dimerization and Lift-off of the Prisms on the Bilayer. SSLBMs in these experiments were prepared by combining a 1:1 mixture of TP-A (Cy5-labeled) and TP-B (Cy3-labeled) and anchoring them together on the beads. Figure 9B, row 1 shows representative confocal microscopy images of the beads in the two Cy3/Cy5 fluorescent channels.

Initial experiments confirmed that each individual prism population can be addressed within this mixed prism bilayer. In Figure 9B row 2, the cholesterol-labeled displacement strand for prism TP-A is added, and the images show bead fluorescence only in the Cy3 channel, consistent with TP-A removal. Row 3 shows the selective lift-off of prism TP-B and disappearance of the Cy3 fluorescence. Finally in row 4 both of the displacement strands are added, and we observe complete loss of fluorescence as both of the prism groups are released from the bilayer surface. Analysis of the fluorescence intensity of the beads, as monitored during the displacement and prism removal events, are shown in Figure 9A and correlate with the captured images.

We then added an equimolecular amount of linking strand to these SSLBMs in order to induce prism dimerization (Figure 10, row 1). Successfully dimerized prisms should contain 2 cholesterol anchor points to the bilayer. If only a single DNA-cholesterol anchor is displaced, the remaining anchor may continue to hold the assembly on the bilayer. Figure 10 rows 2 and 3 show the results of performing a single anchor displacement on the dimerized DNA cages. When either TP-A or TP-B is addressed with its specific anchor displacement strand, we see that the beads remain fluorescent in both label channels. Quantitative analysis, Figure 11, carried out for

dx.doi.org/10.1021/ja506095n | J. Am. Chem. Soc. 2014, 136, 12987−12997

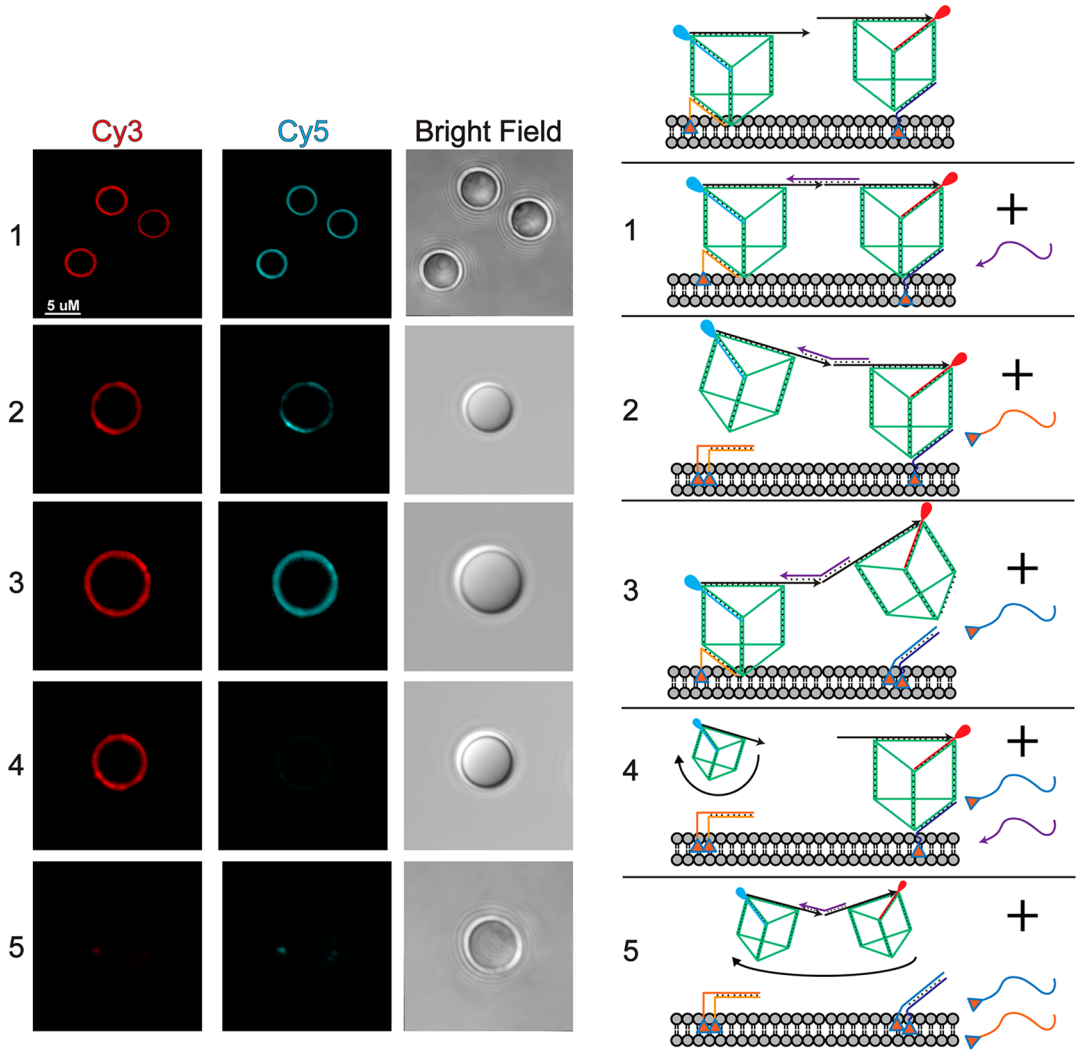

Figure 10. Confocal fluorescent images of dimerization and lift-off of the prisms on the bilayer: (1) control sample TP-A(Cy5) + TP-B(Cy3) with linker. (2) Displace TP-A (Cy5). (3) Displace TP-B (Cy3). (4) Displace TP-B (Cy3) and add the linker displacement strand to break the dimer. (5) Displace dimer prisms by adding both cholesterol erasing strands.

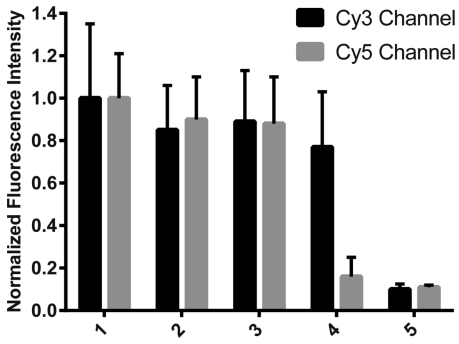

Figure 11. Normalized fluorescence intensity measurements for rows 1 to 6 from Figure 11.

sample populations of at least 50 beads shows that the ratio of Cy3:Cy5 fluorescence is maintained, in agreement with the continued presence of the prism dimer that is now singly anchored.

If the resulting prism dimer is singly anchored, then addition of the linker displacement strand should dissociate it into the two prism monomers, thus liberating the nonanchored prism component, which can be removed upon washing. Figure 10 row 4 shows the reaction sequence in which the anchor of TP-A is first displaced, followed by linker displacement. Indeed, only the Cy3 fluorescence for TP-B remains on the beads, consistent with dissociation of the prism dimer into monomers and removal of TB-P after washing.

The dimerized prism could only be lifted off into the supernatant when DNA-cholesterol anchor displacement strands for both component prisms were added (Figure 10 row 5). Quantitative analysis shows only a residual (10%) fluorescence remaining on the beads in either Cy3 or Cy5 channels (Figure 11). The supernatant was collected after bead centrifugation. PAGE analysis indeed reveals the formation of a prism dimer, which can be separated into the two prism monomers upon displacement of the linking strand (Supporting Information, Figure S8).

■ CONCLUSIONS

These experiments have clearly shown that amphiphilic DNA cages can retain their dynamic behavior when associated with a supported bilayer membrane environment. The anchored DNA cage can load and selectively unload three different DNA-fluorophores on its top face via strand displacement. On the

dx.doi.org/10.1021/ja506095n | J. Am. Chem. Soc. 2014, 136, 12987−12997

other hand, displacement of the cage from the bottom prism face required functionalization of the erasing strand with a cholesterol group. This addition renders the erasing strand more soluble within the bilayer. It is thus be able to adopt a favorable orientation with which to access the toehold region for displacement.

The DNA scaffolds were also tunable in terms of their orientation within a bilayer environment. This parameter was controlled by positioning multiple cholesterol anchors on the two faces of the DNA cage, thus changing its orientation within the SSLBMs. The resulting embedded cages were less susceptible to DNase I degradation, suggesting that access of anchored cages to proteins is tunable through site-specific modification of the cages themselves. This finding introduces new strategies to protect DNA cages from protein binding and nuclease degradation, when used in drug delivery applications.

Finally, we demonstrated the successful association of two different prisms by hybridization on-bilayer. The resulting dimer prism can only be released from the bilayer when both of its anchored prisms components are displaced, but stays associated with the bilayer if only one of its components is displaced.

The DNA cage used here is the simplest 3D object that we can form via our clip-by-clip assembly. We have shown that this 3D-assembly method is highly modular, allowing us to combine up to eight clipping strands into octameric prisms, which contain 16 asymmetric ss regions available for hybridization with various DNA conjugates (unpublished material). Unlike DNA origami constructs, the DNA cages appear to be intimately coupled to the lipid bilayer, which sterically blocks access to one or more of their sites. This will have interesting consequences on their ability for tunable cellular penetration and protein binding.

Overall, this approach allows stable association of DNA cages with lipid bilayers, controlling their orientation and accessibility within the membrane, bringing them together by hybridization and selectively lifting off any of their components. These events will potentially allow programmable dynamic control of protein binding, cell signaling, drug delivery, nanoelectronic and optical properties on lipid bilayers using a modular, easy to construct and DNA-economic scaffold.

■ ASSOCIATED CONTENT

Ⓢ Supporting Information

Oligonucleotide synthesis and characterization, DNA cage assembly and functionalization, preparation of cage-anchored SSLBMs, bilayer loading quantification, confocal microscopy, FRAP experiments. This material is available free of charge via the Internet at http://pubs.acs.org.

■ AUTHOR INFORMATION

Corresponding Author

hanadi.sleiman@mcgill.ca

Notes

The authors declare no competing financial interest.

■ ACKNOWLEDGMENTS

We would like to thank FQRNT, NSERC, CFI, CIHR, and CSACS for financial support. H.F.S. is a Cottrell scholar of the Research Corporation.

■ REFERENCES

(1) (a) Borjesson, K.; Wiberg, J.; El-Sagheer, A. H.; Ljungdahl, T.; Martensson, J.; Brown, T.; Norden, B.; Albinsson, B. *ACS Nano* **2010**, *4*, 5037−5046. (b) Howorka, S. *Langmuir* **2013**, *29*, 7344−7353. (c) Kwak, M.; Herrmann, A. *Chem. Soc. Rev.* **2011**, *40*, 5745−5755. (d) van der Meulen, S. A. J.; Leunissen, M. E. *J. Am. Chem. Soc.* **2013**, *135*, 15129−15134.

(2) (a) He, H. Z.; Chan, D. S. H.; Leung, C. H.; Ma, D. L. *Nucleic Acids Res.* **2013**, *41*, 4345−4359. (b) Leung, C. H.; Chan, D. S. H.; He, H. Z.; Cheng, Z.; Yang, H.; Ma, D. L. *Nucleic Acids Res.* **2012**, *40*, 941−955. (c) Ma, D. L.; He, H. Z.; Chan, D. S. H.; Leung, C. H. *Chem. Sci.* **2013**, *4*, 3366−3380. (d) Ma, D. L.; He, H. Z.; Leung, K. H.; Zhong, H. J.; Chan, D. S. H.; Leung, C. H. *Chem. Soc. Rev.* **2013**, *42*, 3427−3440.

(3) Hung, Y. C.; Lin, T. Y.; Hsu, W. T.; Chiu, Y. W.; Wang, Y. S.; Fruk, L. *Opt. Mater.* **2012**, *34*, 1208−1213.

(4) (a) Jones, M. R.; Osberg, K. D.; Macfarlane, R. J.; Langille, M. R.; Mirkin, C. A. *Chem. Rev.* **2011**, *111*, 3736−3827. (b) Pal, S.; Dutta, P.; Wang, H. N.; Deng, Z. T.; Zou, S. L.; Yan, H.; Liu, Y. *J. Phys. Chem. C* **2013**, *117*, 12735−12744. (c) Young, K. L.; Ross, M. B.; Blaber, M. G.; Rycenga, M.; Jones, M. R.; Zhang, C.; Senesi, A. J.; Lee, B.; Schatz, G. C.; Mirkin, C. A. *Adv. Mater.* **2014**, *26*, 653−659.

(5) (a) Keum, J. W.; Ahn, J. H.; Bermudez, H. *Small* **2011**, *7*, 3529−3535. (b) Li, J.; Pei, H.; Zhu, B.; Liang, L.; Wei, M.; He, Y.; Chen, N.; Li, D.; Huang, Q.; Fan, C. H. *ACS Nano* **2011**, *5*, 8783−8789. (c) Schuller, V. J.; Heidegger, S.; Sandholzer, N.; Nickels, P. C.; Suhartha, N. A.; Endres, S.; Bourquin, C.; Liedl, T. *ACS Nano* **2011**, *5*, 9696−9702.

(6) (a) Walsh, A. S.; Yin, H. F.; Erben, C. M.; Wood, M. J. A.; Turberfield, A. J. *ACS Nano* **2011**, *5*, 5427−5432. (b) Hamblin, G. D.; Carneiro, K. M.; Fakhoury, J.; Bujold, K. E.; Sleiman, H. F. *J. Am. Chem. Soc.* **2012**, *134*, 2888−2891. (c) Fakhoury, J.; McLaughlin, C.; Edwardson, T.; Conway, J.; Sleiman, H. F. *Biomacromolecules* **2014**, *15*, 276−282.

(7) Park, S. Y.; Lytton-Jean, A. K. R.; Lee, B.; Weigand, S.; Schatz, G. C.; Mirkin, C. A. *Nature* **2008**, *451*, 553−556.

(8) (a) Banchelli, M.; Betti, F.; Berti, D.; Caminati, G.; Bombelli, F. B.; Brown, T.; Wilhelmsson, L. M.; Norden, B.; Baglioni, P. *J. Phys. Chem. B* **2008**, *112*, 10942−10952. (b) Beales, P. A.; Vanderlick, T. K. *J. Phys. Chem. B* **2009**, *113*, 13678−13686.

(9) Chung, M.; Boxer, S. G. *Langmuir* **2011**, *27*, 5492−5497.

(10) (a) Chan, Y. H. M.; van Lengerich, B.; Boxer, S. G. *Biointerphases* **2008**, *3*, FA17. (b) Stengel, G.; Zahn, R.; Hook, F. *J. Am. Chem. Soc.* **2007**, *129*, 9584−9585.

(11) Li, C. Y.; Wood, D. K.; Hsu, C. M.; Bhatia, S. N. *Lab Chip* **2011**, *11*, 2967−2975.

(12) (a) Burns, J. R.; Stulz, E.; Howorka, S. *Nano Lett.* **2013**, *13*, 2351−2356. (b) Langecker, M.; Arnaut, V.; Martin, T. G.; List, J.; Renner, S.; Mayer, M.; Dietz, H.; Simmel, F. C. *Science* **2012**, *338*, 932−936.

(13) Woller, J. G.; Hannestad, J. K.; Albinsson, B. *J. Am. Chem. Soc.* **2013**, *135*, 2759−2768.

(14) Schade, M.; Knoll, A.; Vogel, A.; Seitz, O.; Liebscher, J.; Huster, D.; Herrmann, A.; Arbuzova, A. *J. Am. Chem. Soc.* **2012**, *134*, 20490−20497.

(15) (a) Suzuki, Y.; Endo, M.; Yang, Y. Y.; Sugiyama, H. *J. Am. Chem. Soc.* **2014**, *136*, 1714−1717. (b) Johnson-Buck, A.; Jiang, S.; Yan, H.; Walter, N. G. *ACS Nano* **2014**, *8*, 5641−5649. (c) Langecker, M.; Arnaut, V.; List, J.; Simmel, F. C. *Acc. Chem. Res.* **2014**, *47*, 1807−1815.

(16) Czogalla, A.; Petrov, E. P.; Uzunova, V.; Zhang, Y.; Seidel, R.; Schwille, P. *Faraday Discuss.* **2013**, *161*, 31−43.

(17) Conway, J. W.; McLaughlin, C. K.; Castor, K. J.; Sleiman, H. *Chem. Commun.* **2013**, *49*, 1172−1174.

(18) Lo, P. K.; Karam, P.; Aldaye, F. A.; McLaughlin, C. K.; Hamblin, G. D.; Cosa, G.; Sleiman, H. F. *Nat. Chem.* **2010**, *2*, 319−328.

(19) Bayerl, T. M.; Bloom, M. *Biophys. J.* **1990**, *58*, 357−362.

(20) Mornet, S.; Lambert, O.; Duguet, E.; Brisson, A. *Nano Lett.* **2005**, *5*, 281−285.

(21) (a) Tanaka, M.; Sackmann, E. *Nature* **2005**, *437*, 656−663. (b) Argyo, C.; Weiss, V.; Bräuchle, C.; Bein, T. *Chem. Mater.* **2014**, *26*, 435−451.
(22) Gopalakrishnan, G.; Thostrup, P.; Rouiller, I.; Lucido, A. L.; Belkaid, W.; Colman, D. R.; Lennox, R. B. *ACS Chem. Neurosci.* **2010**, *1*, 86−94.
(23) Schwille, P.; Diez, S. *Crit. Rev. Biochem. Mol.* **2009**, *44*, 223−242.
(24) (a) Troutier, A. L.; Ladaviere, C. *Adv. Colloid Interface Sci.* **2007**, *133*, 1−21. (b) Gopalakrishnan, G.; Rouiller, I.; Colman, D. R.; Lennox, R. B. *Langmuir* **2009**, *25*, 5455−5458.
(25) (a) Borjesson, K.; Lundberg, E. P.; Woller, J. G.; Norden, B.; Albinsson, B. *Angew. Chem. Int. Ed.* **2011**, *50*, 8312−8315. (b) Woller, J. G.; Borjesson, K.; Svedhem, S.; Albinsson, B. *Langmuir* **2012**, *28*, 1944−1953.